ACS OMEGA

http://pubs.acs.org/journal/acsodf

Article

Anisotropic Growth of Copper Nanorods Mediated by Cl^- Ions

Min Jia Saw, Mai Thanh Nguyen,* Yuji Kunisada, Tomoharu Tokunaga, and Tetsu Yonezawa*

Cite This: *ACS Omega* 2022, 7, 7414–7420

Read Online

ACCESS | Metrics & More | Article Recommendations | Supporting Information

ABSTRACT: Anisotropic growth to form Cu particles of rod and wire shapes has been obtained typically in a complex system that involves both organic capping agents and Cl^- ions. However, the sole effect of Cl^- ions on the formation of Cu wires has yet to be fully understood, especially in an organic system. This present work determines the effect of Cl^- ions on the morphologies of Cu particles in an organic phase without any capping agents. The results revealed that anisotropic Cu rods could be grown with the sole presence of Cl^- ions. The rods have the (011) facets as the long axis, the (111) facets as the tip, and the (100) facets as the side surface. By increasing the Cl^- ion concentration, more Cu atoms contributed to the formation of Cu rods and the kinetic growth of the length and the diameter of the rods varied. This suggests that Cl^- ions have preferential adsorption on the (100) Cu surfaces to promote the anisotropic growth of Cu. Meanwhile, the adsorption of Cl^- to the (111) and (100) surfaces at high Cl^- concentrations regulates the relative growth of the particle length and diameter.

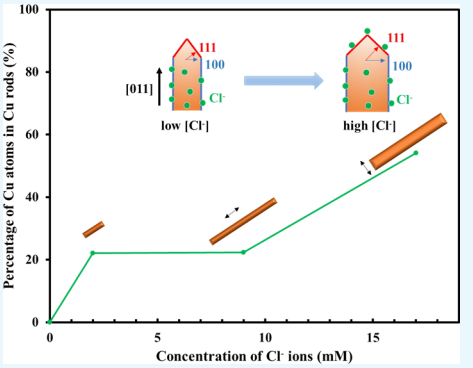

1. INTRODUCTION

Metallic fine particles have been intensively researched for several decades.[1−13] Among the metals available, copper (Cu) is of great interest because it is non-expensive, abundant, and non-toxic and has impressive properties such as good conductivity, good catalytic properties, and anti-electromigration.[14−40] Cu particles with different morphologies and sizes have been used in many industries. For example, Cu fine particles are widely applied in printing electronic fields[14−18] and Cu nanoparticles are broadly used as catalysts[19−22] while Cu nanowires are popular as transparent conducting electrode materials.[23−40]

While there are many methods on preparing the Cu particles, chemical synthesis is a favorable method because this method is cost-effective, requires a simple equipment setup, and can manipulate the size and shape of the synthesized particles.[41] In a typical chemical synthesis of Cu particles, the formation of different morphologies of Cu particles is generally governed by the initial geometry of the seeds and the preference of capping agents (*i.e.*, shape-directing agents) to be adsorbed on certain facets of the nanocrystal to control the growth of the facets.[30,38−40,42−49,51] A cuboctahedron seed grows into a sphere if the growth rates of all facets are the same.[43,44] When the adsorption affinity of the surfactants is stronger in a certain facet of the cuboctahedron seed, for instance, on the (100) surface, the growth rate of the (111) surface is then higher, leading to the formation of a cubic-shaped particle.[42−44] On the other hand, if the initial seed is a decahedron seed particle, the growth rate of the (111) surface is higher than that of the (100) surface, leading to the elongation of the seed into a rod-shaped or wire-shaped particle.[38,42−49]

The ability to synthesize Cu particles with tunable sizes and shapes could improve the application of the Cu particles in various fields.[14−40] Peculiarly, Cu nanowires are widely studied as one-dimensional nanostructures for achieving high conductivity and optical transparency when using Cu as transparent conducting materials.[23−40] While the directing agents such as polyvinylpyrrolidone (PVP) or amines (e.g., 1-hexadecylamine (HDA) and ethylenediamine (EDA)) play an important role in controlling the morphology of Cu nanowires, the existence of Cl^- ions is also deemed as necessary for most of the synthesis method available.[42,44−49] Regardless, the exact role of Cl^- ions in the formation of one-dimensional structured Cu particles is yet to be fully understood, especially in an organic phase since the syntheses often involve a complex system.[45,50] With a better understanding on how Cl^- ions solely affect the morphologies of Cu particles, especially for the growth of Cu wires and rods in an organic system, the strategy to tune the morphologies of Cu could be further improved. We hereby design a simple synthesis system in ethylene glycol (EG) without using organic shape-directing agents to study the sole effect of Cl^- ions on the morphologies of Cu particles.

Received: January 18, 2022
Accepted: February 3, 2022
Published: February 16, 2022

https://doi.org/10.1021/acsomega.2c00359
ACS Omega 2022, 7, 7414−7420

2. RESULTS AND DISCUSSION

Cu particles were synthesized in a system without organic capping agents. The Cu particles were prepared by reducing a Cu complex in EG using ascorbic acid (AsA) with various Cl^- concentrations, 0−17 mM, as shown in Figure 1.

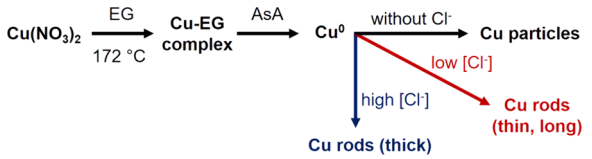

Figure 1. Scheme of the synthesis of Cu particles and Cu rods of different sizes without and with using Cl^-, respectively.

The samples obtained in these syntheses are labeled according to the Cl^- concentration in the final reaction solution, i.e., samples Cl_0, Cl_2, Cl_9, Cl_17_20h, and Cl_17_42h. Figure 2 shows the XRD data of the synthesized

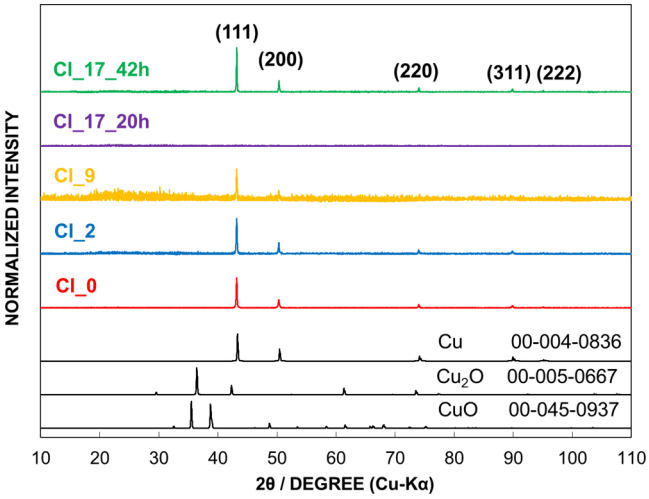

Figure 2. XRD patterns of the Cu fine particles that were synthesized with different concentrations of Cl^- ions and the reference patterns of Cu (JCPDS no. 004-0836), CuO (JCPDS no. 045-0937), and Cu_2O (JCPDS no. 005-0667).

Cu particles with different concentrations of Cl^- ions. The Cu particles for the samples Cl_0, Cl_2, Cl_9, and Cl_17_42h have peaks in 2θ at 43.30, 50.43, 74.13, 89.93, and 95.14°, identical with that in the reference pattern of Cu (JCPDS no. 004-0836). No oxide peaks were detected, indicating that the samples are metallic Cu. For samples Cl_0, Cl_2, and Cl_9, the Cu peaks were observed after 20 h reaction time. However, for the sample Cl_17_20h, Cu peaks were not detected after 20 h reaction time. By prolonging the reaction time to 42 h (sample Cl_17_42h), the Cu peaks were observed, indicating that Cu was reduced. This result suggests that by increasing the amount of Cl^- ions, it is harder for the Cu complex to be reduced to Cu, and hence, a longer reaction time is needed for the reduction of Cu.

The morphologies of the Cu fine particles were determined by SEM images (Figure 3). In sample Cl_0 (Figure 3a), when there is no Cl^- ions, the sample consists only of particles in various shapes (term as "other shapes" in this paper) such as triangles, pentagons, hexagons, and cubes (Figure S1). No rods or wires were observed. For sample Cl_2 (Figure 3b), when

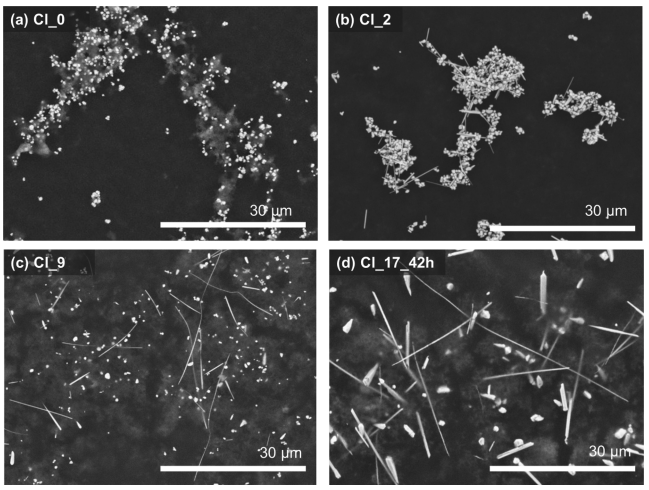

Figure 3. SEM images of the Cu fine particles that were synthesized with Cl^- concentrations of (a) 0, (b) 2, (c) 9, and (d) 17 mM (42 h reaction).

the Cl^- ion concentration increases to 2 mM, few short rods with an average length of 4.3 μm and an average diameter around 261 nm (aspect ratio ~16.2) were observed, along with the Cu particles of other shapes. The results prove that Cl^- ions are needed for the anisotropic growth of Cu to a rod-shaped structure. In previous studies, nanowires were observed when Cl^- ions existed in the reaction system along with other capping agents such as PVP and HDA.[42,44−48,50] In our study, without using any organic capping agents, we can confirm the sole effect of Cl^- ions in directing the anisotropic growth of Cu to a rod shape. By further increasing the concentration of Cl^- ions to 9 mM in sample Cl_9 (Figure 3c and Figure S2), similarly, the Cu rods and Cu particles of other shapes were observed. However, the Cu rods grow longer with an average length of 12.8 μm and an average diameter around 224 nm. The aspect ratio of the Cu rods is improved to ~57.4. For the sample Cl_17_42h (Figure 3d and Figure S3), both Cu rods and Cu particles of other shapes were also observed. The average length of Cu rods increases slightly to 15.4 μm, while the average diameter increases twice to around 409 nm, resulting in a shorter aspect ratio (~37.5) than sample Cl_9. Table 1 summarizes the average diameter, the average length,

Table 1. Dimensions of Cu Rods with Different Cl^- Concentrations in the Reaction Solution

sample	[Cl^-] (mM)	diameter (nm)	length (μm)	aspect ratio
Cl_0	0	NA	NA	NA
Cl_2	2	261.0 ± 95.2	4.3 ± 1.9	~16.2
Cl_9	9	224.1 ± 59.8	12.8 ± 7.2	~57.4
Cl_17_42h	17	409.6 ± 123.4	15.4 ± 6.5	~37.5

and the corresponding aspect ratios of Cu rods for all concentrations of Cl^- ions. Based on the observations for samples Cl_2 and Cl_9, it is obvious that initially, the length of Cu rods increases when there is more Cl^- ions in the reaction. However, by further increasing the concentration of Cl^- ions, the length of rods only increases slightly, while the diameter of Cu rods continues to increase, as observed in the Cl_17_42h sample. In a previous report where the Cl^- ion concentration was increased in a three-phase system with colloidal templates (surfactant), the diameter of Cu nanorods increased while the

https://doi.org/10.1021/acsomega.2c00359
ACS Omega 2022, 7, 7414−7420

length reached a maximum (with an aspect ratio around 12).[50] However, the length of Cu rods in our case kept increasing slightly rather than reaching a maximum and the aspect ratio in our case is higher (~37). Our results imply that when Cl^- ions exist at low concentrations in the system, the growth of the length of Cu rods is preferable. However, with more Cl^- ions, the growth of the diameter speeded up relative to that of the length. Overall, at a high Cl^- concentration, the aspect ratio of the rod was smaller.

Without any effect from other organic capping agents in EG, it is obvious that Cl^- ions are pivotal in the anisotropic growth and formation of Cu rods. To understand the role of Cl^- ions in the growth of Cu rods more deeply, we compared the percentage of Cu atoms that contribute to form the rods aside from the percentage of the number of Cu rods among the samples. Since the synthesized Cu rods and Cu particles of other shapes have different volumes due to their morphologies, it is significant to compare the percentages of the morphologies in terms of the number of Cu atoms rather than simply counting the number of particles for each morphology. The details on the calculation method and results are shown in the Supporting Information (Figure S4, Tables S1 and S2, and Appendix S1). The results are plotted and shown in Figure 4.

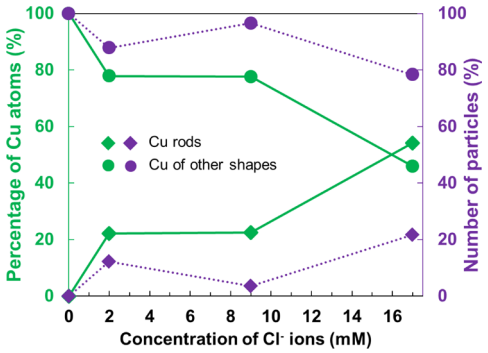

Figure 4. (left *y*-axis) Percentages of Cu atoms contributing to Cu rods and Cu particles of other shapes and (right *y*-axis) number of Cu particles of rod shape and other shapes with different concentrations of Cl^- ions.

When 2 mM Cl^- ions was used in the reaction solution, 22.2% of Cu atoms formed the rods, resulting in 12.2% Cu rods in the sample. When the concentration of Cl^- ions was 9 mM, even though the number of resulting Cu rods is lesser (3.4%), in fact, more Cu atoms (22.4%) contributed to the formation of the rods with the highest aspect ratio. On the other hand, with 17 mM Cl^- ions, 54.1% of Cu atoms contributed to the formation of Cu rods, resulting in the number of Cu rods being 21.7%. These results clearly show that Cl^- ions could enhance the formation of the anisotropic rod-shaped structure of Cu, as there were more Cu atoms involved in the formation of rods when more Cl^- ions existed in the system.

We further analyzed SAED patterns coupled with the TEM images of Cu rods to understand the particle growth. The bright spots in the SAED pattern (Figure 5b) of the Cu rod shown in the TEM image (Figure 5a) were indexed to the diffraction from the (111) and (200) planes of Cu, confirming the fcc structure. Furthermore, the SAED result and the TEM image reveal that the Cu rod grows along the [011] direction with the (100) facets toward the side of the rod. The tip surface is normal to the [111] direction (Figure 5c), suggesting that the facets on the tip are the (111) planes. We noticed that

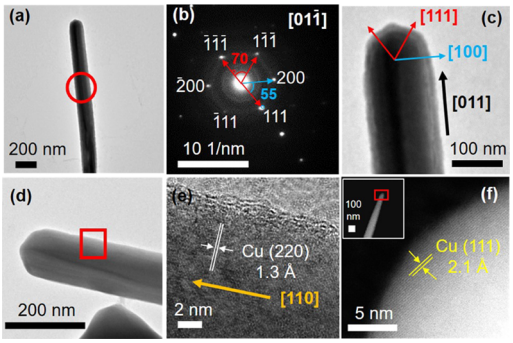

Figure 5. (a) TEM image of a Cu rod with (b) its corresponding SAED pattern taken at the area marked with a circle in the TEM image. (c) Directions on the side and the tip facets of the rod. (d) TEM image of another Cu rod and (e) HRTEM image of the side of the rod (marked with a red square in (d)), confirming that the rod grew in the [110] direction, which is equivalent to [011] in the fcc structure. (f) STEM-HAADF image showing the (111) facets at the tip of a Cu rod, which is marked with a red square in the inset of (f).

the defects such as twin planes or twisted areas could be present in the rods, as observed in the TEM images with areas of darker contrast. The growth direction and facets of Cu rods are further confirmed by HRTEM and HAADF images (Figure 5d–f) where the (220) planes along the rod and the (111) facets at the tip were clearly visible. On the other hand, Cu particles of other shapes consist of facets that are either (111) or (200) (Figures S5 and S6). This suggests that the kinetics of all facets are more similar for the case of Cu particles, which does not lead to elongated structures. EELS analysis (Figure S7) was performed on the side (Figure S7a) and tip (Figure S7b) of the Cu rods. At both the inner and outer areas of the side of the rod (areas 1 and 2), the spectra showed L_3 (200 eV) and L_2 (202 eV) edges of Cl, suggesting the presence of Cl on the (100) facets. In contrast, the edges of Cl were only detected for the inner area of the tip. These observations suggest that Cl^- ions have a stronger preferential adsorption on the (100) facets of Cu than the (111) facets. DFT simulation results (Table 2) showed that the adsorption of Cl on the

Table 2. Adsorption Energy of Cl on Cu Surfaces Obtained from Simulation

Cu surface	super cell size	coverage of Cl (atom/nm^2)	adsorption energy (eV)
(100)	2 × 2	1.9	−3.4
(100)	1 × 1	7.6	−3.3
(111)	2 × 2	4.4	−3.2
(111)	1 × 1	13.6	−0.7

Cu(100) surface is more preferable than that on the Cu(111) surface. This is consistent with the experimental results. Since Cl^- ions have a stronger adsorption on the (100) facets, the addition of Cu atoms on these facets will be delayed. During growth, Cu atoms continue to add to the (111) facets, leading to the elongation of rods in the [011] direction. At high concentrations of Cl^- (i.e., sample Cl_17_42h), Cl^- ions can be more involved in the adsorption to the (111) facets, causing less difference in the growth rate between the (111) and (100) planes. This explains the growth of Cu rods with a thicker diameter. Figure 6 illustrates the preferential adsorption of Cl^- ions on Cu facets for the anisotropic growth of Cu rods at low

https://doi.org/10.1021/acsomega.2c00359
ACS Omega 2022, 7, 7414−7420

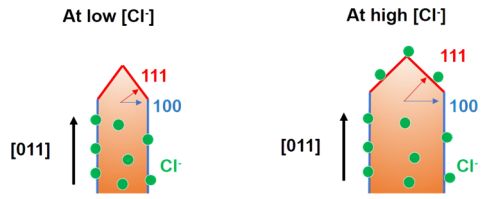

Figure 6. Schematic showing the preferential adsorption of Cl^- ions on the Cu facets for the growth of the rods in the length (left) and diameter (right) depending on the Cl^- concentration.

and high Cl^- concentrations for the growth of the length and the diameter of the rods.

3. EXPERIMENTAL SECTION

3.1. Materials. Copper(II) nitrate trihydrate ($Cu(NO_3)_2.3H_2O$, Kanto, Japan), ethylene glycol (EG, Kanto), sodium chloride (NaCl, Wako), ascorbic acid (AsA, Kanto), and methanol (MeOH, Wako) were used as received.

3.2. Synthesis of Cu Fine Particles. Cu particles were synthesized by using a chemical reduction method (Figure 7).

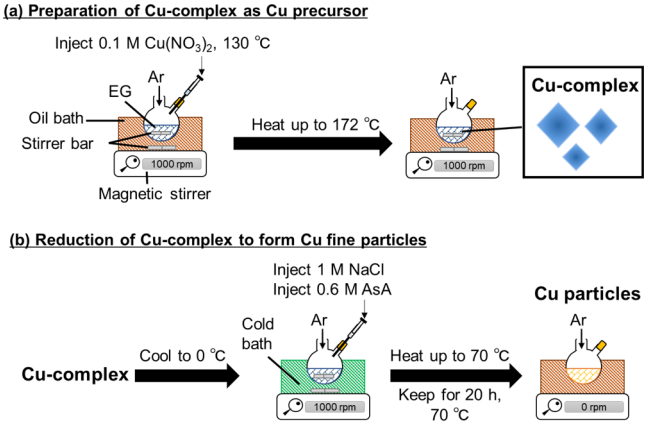

Figure 7. Synthesis procedure of Cu fine particles.

The synthesis consists of two steps: preparation of the Cu complex as a Cu precursor and reduction of the Cu complex to form Cu particles.

(a) Preparation of Cu-complex as a Cu precursor

First, 100 mL of EG was added into a two-neck Kjeldahl-shaped flask and heated at 130 °C for 1 h under an argon atmosphere with magnetic stirring at 1000 rpm. Simultaneously, $Cu(NO_3)_2$ solution (0.1 M, in EG) was prepared. Then, 10 mL of $Cu(NO_3)_2$ solution was injected into the preheated EG solution and left stirring for 15 min. Subsequently, the reaction solution was heated to 172 °C to form the Cu complex with EG. The reaction solution was quenched down immediately once the solution turned to opaque blue, an indication of the formation of the Cu complex (Figure S8).

(b) Reduction of the Cu complex to form Cu fine particles

NaCl solution (1 M, in EG) and AsA solution (0.6 M, in EG) were prepared. The Cu-complex solution was cooled down to 0 °C under vigorous magnetic stirring. Subsequently, in a typical synthesis, 1 mL of NaCl solution was injected into the reaction solution and stirred for 15 min followed by the injection of 5 mL of AsA solution and 15 min vigorous stirring. The solution was then heated in an oil bath to 70 °C and left reacting for 20 h without stirring. Finally, the reaction solution was quenched down to room temperature and centrifuged twice at 3000 rpm for 10 min with MeOH. The purified Cu particles were dispersed in MeOH for further characterization. To investigate the impact of Cl^- ions on the morphologies of Cu particles, the volume of the injected 1 M NaCl solution was varied (0, 0.25, 1, and 2 mL), which resulted in the final Cl^- concentrations of 0, 2, 9, and 17 mM, respectively, in the reaction solution. The samples obtained in these syntheses are labeled according to the Cl^- concentration in the final reaction solution, i.e., samples Cl_0, Cl_2, Cl_9, Cl_17_20h, and Cl_17_42h. The same procedures were carried out for each synthesis, and the detailed parameters are summarized in Table 3.

3.3. Characterization. The crystalline and phase structures of Cu particles were characterized using X-ray diffraction (XRD, Rigaku Miniflex II X-ray diffractometer, Cu Kα radiation, λ = 1.5418 Å, scanning speed of 10° min^{-1}). The morphologies and selective area electron diffraction (SAED) images of the synthesized Cu particles were examined using scanning electron microscopes (SEM, JEOL-JSM-6701F and Hitachi TM3030 Plus, 15 kV) and transmission electron microscopes (TEM, JEOL JEM-2000FX, 200 kV and JEOL JEM-2010, 200 kV), respectively. High-resolution (HR)TEM and high-angle annual dark-field (HAADF) images and electron energy loss spectra (EELS) were acquired using a scanning TEM (STEM, ARM200F, 200 kV). The TEM sample was prepared by adding a drop of Cu particle dispersion onto a molybdenum TEM grid. The average particle size of Cu particles was measured based on SEM and TEM images.

3.4. DFT Calculation. DFT calculation was carried out for the Cu(111) and Cu(100) surfaces with 1 × 1 and 2 × 2 supercells to vary the coverage of Cl. The supercell consisted of a single Cl atom and periodically repeated five Cu atomic layers with a 15 Å vacuum layer. We performed DFT calculations using the Vienna ab initio Simulation Package (VASP 5.4.4)[52−55] and the projector-augmented wave (PAW) method.[56,57] We adopted the generalized gradient approximation proposed by Perdew, Burke, and Ernzerhof[58] as an exchange−correlation functional. The plane-wave basis set was used with an energy cutoff of 400 eV. We used 16 × 16 × 1, 8 × 8 × 1, 12 × 12 × 1, and 6 × 6 × 1 Γ-point centered

Table 3. Amount of EG, $Cu(NO_3)_2$, NaCl, and AsA Used for Each Synthesis

		injected solution			reaction solution		
sample	EG before injection (mL)	0.1 M $Cu(NO_3)_2$ (mL)	1 M NaCl (mL)	0.6 M AsA (mL)	total EG (mL)	$[Cl^-]$ (mM)	reaction time (h)
Cl_0	100	10	0	5	115.00	0	20
Cl_2	100	10	0.25	5	115.25	2	20
Cl_9	100	10	1.00	5	116.00	9	20
Cl_17_20h	100	10	2.00	5	117.00	17	20
Cl_17_42h	100	10	2.00	5	117.00	17	42

https://doi.org/10.1021/acsomega.2c00359
ACS Omega 2022, 7, 7414−7420

Monkhorst–Pack grids[59] for Brillouin zone sampling with a Gaussian smearing σ of 0.2 eV for the 1 × 1 Cu(111), 2 × 2 Cu(111), 1 × 1 Cu(100), and 2 × 2 Cu(100) surfaces, respectively. The top three Cu atomic layers and Cl atoms were fully relaxed until the force on each atom was less than 0.02 eV/Å. We adopted fcc-hollow and four-fold hollow sites as the Cl adsorption sites for the Cu(111) and Cu(100) surfaces. We defined the adsorption energies of the Cl atom on Cu surfaces E_{ad} using the following equation:

$$E_{ad} = E_{Cl/Cu} - [E_{Cu} + E_{Cl}] \quad (1)$$

where $E_{Cl/Cu}$, E_{Cu}, and E_{Cl} are the total energies of Cl-adsorbed Cu surfaces, clean Cu surfaces, and isolated Cl atoms, respectively. The minus sign of the adsorption energy means that Cl adsorbed on the Cu surface. The absolute value indicates the strength of the adsorption.

4. CONCLUSIONS

This research demonstrates that without organic capping agents in the system, Cl^- ions are needed for the anisotropic growth of Cu rods. The concentration of Cl^- ions affects the number of Cu atoms that contribute to the formation of Cu rods, the aspect ratio, and the particle number percentage of the rods. At a low Cl^- concentration, the Cl^- ions have a stronger adsorption affinity on the (100) facets of Cu, leaving the (111) facets to grow faster and forming Cu rods along the [011] direction. On the other hand, at a high Cl^- concentration, the growth of the (111) facets become less preferable in comparison to that of the (100) facets, forming thicker rods. This study has provided more insight on the role of Cl^- ions in controlling the anisotropic growth of Cu in the absence of organic capping agents.

■ ASSOCIATED CONTENT

Supporting Information

The Supporting Information is available free of charge at https://pubs.acs.org/doi/10.1021/acsomega.2c00359.

SEM images of Cu fine particles of samples Cl_0, Cl_9 (at low magnification), and Cl_17_42h (at low magnification); measurement method on the size of Cu rods and Cu particles of "other shapes"; dimensions of Cu rods and Cu particles of "other shapes" for each Cl^- concentration; calculation method of the percentage of Cu atoms forming Cu rods and Cu particles of "other shapes"; calculations of the percentages of Cu atoms for Cu rods and Cu particles of "other shapes" for each Cl^- concentration; HRTEM images of Cu particles of other shapes (triangle) with their corresponding lattice spacings in various areas; HRTEM images of Cu particles of other shapes (upper: cube; lower: hexagon) with their corresponding lattice spacings in various areas; HAADF images and EELS spectra of Cu rods at different areas ((100) and (111) facets); and photograph and SEM image of the Cu-EG complex (PDF)

■ AUTHOR INFORMATION

Corresponding Authors

Mai Thanh Nguyen − *Division of Materials Science and Engineering, Faculty of Engineering, Hokkaido University, Sapporo 060-8628, Japan;* orcid.org/0000-0001-5436-123X; Email: mai_nt@eng.hokudai.ac.jp

Tetsu Yonezawa − *Division of Materials Science and Engineering, Faculty of Engineering, Hokkaido University, Sapporo 060-8628, Japan;* orcid.org/0000-0001-7371-204X; Email: tetsu@eng.hokudai.ac.jp

Authors

Min Jia Saw − *Division of Materials Science and Engineering, Faculty of Engineering, Hokkaido University, Sapporo 060-8628, Japan;* orcid.org/0000-0001-7167-9696

Yuji Kunisada − *Center for Advanced Research of Energy and Materials, Faculty of Engineering, Hokkaido University, Sapporo 060-8628, Japan;* orcid.org/0000-0001-7743-5369

Tomoharu Tokunaga − *Department of Materials Science and Engineering, Graduate School of Engineering, Nagoya University, Nagoya 464-8603, Japan*

Complete contact information is available at: https://pubs.acs.org/10.1021/acsomega.2c00359

Notes

The authors declare no competing financial interest.

■ ACKNOWLEDGMENTS

This work is partially supported by Hokkaido University. The authors thank Dr. Y. Ishida and Mr. H. Tsukamoto (Hokkaido University) for fruitful discussion. We also acknowledge Ms. R. Yokohira, Mr. T. Tanioka, and Ms. N. Hirai for their support in TEM and STEM. The DFT simulation was performed using the facilities of the Supercomputer Center, Institute for Solid State Physics, University of Tokyo. M.J.S. thanks MEXT Scholarship for financial support during her stay in Japan. M.T.N. thanks Young Research Acceleration Project of Hokkaido University, Grant for Basic Science Research Projects from the Sumitomo foundation, and the Kurata Grant awarded by the Hitachi Global Foundation. T.Y. thanks Fund for the Promotion of Joint International Research (Fostering Joint International Research (B)) (18KK0159) from JSPS, Grant-in-Aids from JSPS for Challenging Research (Exploratory) (19K22094), on Innovative areas (Research in a Proposed Research Area) (21H00138), JST Adaptable and Seamless Technology Transfer Program through Target-Driven R&D, and Nippon Sheet Glass Foundation for Materials Science and Engineering. Y.K. thanks JSPS KAKENHI: Grant-in-Aid for Early-Career Scientists, No. 20K15165.

■ REFERENCES

(1) Harish, K. K.; Nagasamy, V.; Himangshu, B.; Anuttam, K. Metallic Nanoparticle: A Review. *Biomed. J. Sci. Tech. Res.* **2018**, *4*, 3765−3775.

(2) Zhu, S.; Nguyen, M. T.; Yonezawa, T. Micro- and nano-encapsulated metal and alloy-based phase-change materials for thermal energy storage. *Nanoscale Adv.* **2021**, *3*, 4626−4645.

(3) Saw, M. J.; Nguyen, M. T.; Zhu, S.; Wang, Y.; Yonezawa, T. Synthesis of Sn/Ag-Sn nanoparticles via room temperature galvanic reaction and diffusion. *RSC Adv.* **2019**, *9*, 21786−21792.

(4) Zhu, S.; Nguyen, M. T.; Tokunaga, T.; Yonezawa, T. Size-Tunable Alumina-Encapsulated Sn-Based Phase Change Materials for Thermal Energy Storage. *ACS Appl. Nano Mater.* **2019**, *2*, 3752−3760.

(5) De Juan, L. M. Z.; Maggay, I. V. B.; Nguyen, M. T.; Liu, W.-R.; Yonezawa, T. β-Sn Nanorods with Active (001) Tip Induced LiF-Rich SEI Layer for Stable Anode Material in Lithium Ion Battery. *ACS Appl. Nano Mater.* **2018**, *1*, 3509−3519.

(6) De Juan, L. M. Z.; Nguyen, M. T.; Ishida, Y.; Yonezawa, T.; Tokunaga, T.; Tsukamoto, H.; Ishida, Y. Structural Control Parameters for Formation of Single-Crystalline β-Sn Nanorods in Organic Phase. *Cryst. Growth Des.* **2017**, *17*, 4554−4562.
(7) Shirai, H.; Nguyen, M. T.; Ishida, Y.; Yonezawa, T. A New Approach for Additive-free Room Temperature Sintering of Conductive Patterns Using Polymer-stabilized Sn Nanoparticles. *J. Mater. Chem. C* **2016**, *4*, 2228−2234.
(8) Saw, M. J.; Ghosh, B.; Nguyen, M. T.; Jirasattayaporn, K.; Kheawhom, S.; Shirahata, N.; Yonezawa, T. High Aspect Ratio and Post-Processing Free Silver Nanowires as Top Electrodes for Inverted-Structured Photodiodes. *ACS Omega* **2019**, *4*, 13303−13308.
(9) Zhu, M.; Nguyen, M. T.; Chau, Y. R.; Deng, L. Yonezawa. Pt/Ag Solid Solution Alloy Nanoparticles in Miscibility Gaps Synthesized by Cosputtering onto Liquid Polymers. *Langmuir* **2021**, *37*, 6096−6105.
(10) Nguyen, M. T.; Wongrujipairoj, K.; Tsukamoto, H.; Kheawhom, S.; Mei, S.; Aupama, V.; Yonezawa, T. Synergistic Effect of the Oleic Acid and Oleylamine Mixed-Liquid Matrix on Particle Size and Stability of Sputtered Metal Nanoparticles. *ACS Sustainable Chem. Eng.* **2020**, *8*, 18167−18176.
(11) Chau, Y. R.; Nguyen, M. T.; Zhu, M.; Romier, A.; Tokunaga, T.; Yonezawa, T. Synthesis of composition-tunable Pd−Cu alloy nanoparticles by double target sputtering. *New J. Chem.* **2020**, *44*, 4704−4712.
(12) Deng, L.; Nguyen, M. T.; Mei, S.; Tokunaga, T.; Kudo, M.; Matsumura, S.; Yonezawa, T. Preparation and Growth Mechanism of Pt/Cu Alloy Nanoparticles by Sputter Deposition onto a Liquid Polymer. *Langmuir* **2019**, *35*, 8418−8427.
(13) Nguyen, M. T.; Yonezawa, T. Sputtering onto a liquid: interesting physical preparation method for multi-metallic nanoparticles. *Sci. Technol. Adv. Mater.* **2018**, *19*, 883−898.
(14) Liu, S.; Tokura, R.; Nguyen, M. T.; Tsukamoto, H.; Yonezawa, T. Surfactant-stabilized copper particles for low-temperature sintering: Paste preparation using a milling with small zirconia beads: Effect of pre-treatment with the disperse medium. *Adv. Powder Technol.* **2020**, *31*, 4570−4575.
(15) Yonezawa, T.; Shi, J.; Tsukamoto, H.; Nguyen, M. T. Size-controlled Preparation of Alkylamine-stabilized Copper Fine Particles from Cupric Oxide (CuO) Micro-particles. *MRS Adv.* **2019**, *4*, 413−418.
(16) Yonezawa, T.; Tsukamoto, H.; Nguyen, M. T. Particle size tuning in scalable synthesis of anti-oxidized copper fine particles by polypeptide molecular weights. *Adv. Powder Technol.* **2017**, *28*, 1966−1971.
(17) Yong, Y.; Nguyen, M. T.; Tsukamoto, H.; Matsubara, M.; Liao, Y.-C.; Yonezawa, T. Effect of decomposition and organic residues on resistivity of copper films fabricated via low-temperature sintering of inks composed of a copper complex and copper particles. *Sci. Rep.* **2017**, *7*, 45150.
(18) Yong, Y.; Yonezawa, T.; Matsubara, M.; Tsukamoto, H. The mechanism of alkylamine-stabilized copper fine particles towards improving the electrical conductivity of copper films at low sintering temperature. *J. Mater. Chem. C* **2015**, *3*, 5890−5895.
(19) Gawande, M. B.; Goswami, A.; Felpin, F.-X.; Asefa, T.; Huang, X.; Silva, R.; Zou, X.; Zboril, R.; Varma, R. S. Cu and Cu-Based Nanoparticles: Synthesis and Applications in Catalysis. *Chem. Rev.* **2016**, *116*, 3722−3811.
(20) Bhagat, M.; Anand, R.; Sharma, P.; Rajput, P.; Sharma, N.; Singh, K. Review—Multifunctional Copper Nanoparticles: Synthesis and Applications. *ECS J. Solid State Sci. Technol.* **2021**, *10*, No. 063011.
(21) C-Flores, B. A.; M-Álvarez, O.; A-Arrocena, M. C.; G-Contreras, R.; A-Figueroa, L.; F-Hernández, J.; A-Torres, L. S. Copper: Synthesis Techniques in Nanoscale and Powerful Application as an Antimicrobial Agent. *J. Nanomater.* **2015**, *2015*, 415238.
(22) Hayashida, H.; Yamauchi, N.; Nakashima, K.; Kobayashi, Y. Synthesis of metallic copper nanoparticles in aqueous solution by surfactant-free reduction and silica coating. *Chem. Pap.* **2020**, *74*, 2813−2820.
(23) Qian, F.; Lan, P. C.; Olson, T.; Zhu, C.; Duoss, E. B.; Spadaccini, C. M.; Han, T. Y.-J. Multiphase separation of copper nanowires. *Chem. Commun.* **2016**, *52*, 11627.
(24) Lah, N. A. C.; Trigueros, S. Synthesis and modelling of the mechanical properties of Ag, Au and Cu nanowires. *Sci. Technol. Adv. Mater.* **2019**, *20*, 225−261.
(25) Won, Y.; Kim, A.; Lee, D.; Yang, W.; Woo, K.; Jeong, S.; Moon, J. Annealing-free fabrication of highly oxidation-resistive copper nanowire composite conductors for photovoltaics. *NPG Asia Mater.* **2014**, *6*, No. e105.
(26) Yoon, H.; Shin, D. S.; Babu, B.; Kim, T. G.; Song, K. M.; Park, J. Control of copper nanowire network properties and application to transparent conducting layer in LED. *Mater. Des.* **2017**, *132*, 66−71.
(27) Xiang, H.; Guo, T.; Xu, M.; Lu, H.; Liu, S.; Yu, G. Ultrathin Copper Nanowire Synthesis with Tunable Morphology Using Organic Amines for Transparent Conductors. *ACS Appl. Nano Mater.* **2018**, *1*, 3754−3759.
(28) Duong, T.-H.; Kim, H.-C. Extremely Simple and Rapid Fabrication of Flexible Transparent Electrodes Using Ultralong Copper Nanowires. *Ind. Eng. Chem. Res.* **2018**, *57*, 3076−3082.
(29) Guo, H.; Lin, N.; Chen, Y.; Wang, Z.; Xie, Q.; Zheng, T.; Gao, N.; Li, S.; Kang, J.; Cai, D.; Peng, D.-L. Copper Nanowires as Fully Transparent Conductive Electrodes. *Sci. Rep.* **2013**, *3*, 2323.
(30) Cui, F.; Yu, Y.; Dou, L.; Sun, J.; Yang, Q.; Schildknecht, C.; Schierle-Arndt, K.; Yang, P. Synthesis of Ultrathin Copper Nanowires Using Tris(trimethylsilyl)silane for High-Performance and Low-Haze Transparent Conductors. *Nano Lett.* **2015**, *15*, 7610−7615.
(31) Kang, C.; Yang, S.; Tan, M.; Wei, C.; Liu, Q.; Fang, J.; Liu, G. Purification of Copper Nanowires To Prepare Flexible Transparent Conductive Films with High Performance. *ACS Appl. Nano Mater.* **2018**, *1*, 3155−3163.
(32) Hwang, C.; An, J.; Choi, B. D.; Kim, K.; Jung, S.-W.; Baeg, K.-J.; Kim, M.-G.; Ok, K. M.; Hong, J. Controlled aqueous synthesis of ultra-long copper nanowires for stretchable transparent conducting electrode. *J. Mater. Chem. C* **2016**, *4*, 1441−1447.
(33) Bhanushali, S.; Ghosh, P.; Ganesh, A.; Cheng, W. 1D Copper Nanostructures: Progress, Challenges and Opportunities. *Small* **2015**, *11*, 1232−1252.
(34) Kumar, D. V. R.; Woo, K.; Moon, J. Promising wet chemical strategies to synthesize Cu nanowires for emerging electronic applications. *Nanoscale* **2015**, *7*, 17195−17210.
(35) Tang, Z.; Shahzad, A.; Kim, W.-S.; Yu, T. Cost-effective aqueous-phase synthesis of long copper nanowires. *RSC Adv.* **2015**, *5*, 83880−83884.
(36) Aziz, A.; Zhang, T.; Lin, Y.-H.; Daneshvar, F.; Sue, H.-J.; Welland, M. E. 1D copper nanowires for flexible printable electronics and high ampacity wires. *Nanoscale* **2017**, *9*, 13104−13111.
(37) Chang, Y.-H.; Lin, T.-J.; Wu, Y.-C.; Fan, S.-W.; Lee, Y.-H.; Lai, Y.-R. Surfactant-assisted galvanic synthesis and growth characteristics of copper nanowires. *Inorg. Chem. Front.* **2019**, *6*, 57−62.
(38) Yang, H.-J.; He, S.-Y.; Tuan, H.-Y. Self-Seeded Growth of Five-Fold Twinned Copper Nanowires: Mechanistic Study, Characterization, and SERS Applications. *Langmuir* **2014**, *30*, 602−610.
(39) Nam, V.; Lee, D. Copper Nanowires and Their Applications for Flexible Transparent Conducting Films: A Review. *Nanomaterials* **2016**, *6*, 47.
(40) Ye, S.; Rathmell, A. R.; Chen, Z.; Stewart, I. E.; Wiley, B. J. Metal Nanowire Networks: The Next Generation of Transparent Conductors. *Adv. Mater.* **2014**, *26*, 6670−6687.
(41) Jamkhande, P. G.; Ghule, N. W.; Bamer, A. H.; Kalaskar, M. G. Metal nanoparticles synthesis: An overview on methods of preparation, advantages and disadvantages, and applications. *J. Drug Deliv. Sci. Technol.* **2019**, *53*, 101174.
(42) Fichthorn, K. A.; Chen, Z. Surface science of shape-selective metal nanocrystal synthesis from first-principles: Growth of Cu nanowires and nanocubes. *J. Vac. Sci. Technol., A* **2020**, *38*, No. 023210.

https://doi.org/10.1021/acsomega.2c00359
ACS Omega 2022, 7, 7414−7420

(43) Mott, D.; Galkowski, J.; Wang, L.; Luo, J.; Zhong, C.-J. Synthesis of Size-Controlled and Shaped Copper Nanoparticles. *Langmuir* **2007**, *23*, 5740−5745.
(44) Fichthorn, K. A.; Chen, Z.; Chen, Z.; Rioux, R. M.; Kim, M. Y.; Wiley, B. J. Understanding the Solution-Phase Growth of Cu and Ag Nanowires and Nanocubes from First Principles. *Langmuir* **2021**, *37*, 4419−4431.
(45) Huaman, J. L. C.; Urushizaki, I. Jeyadevan, B. Large-Scale Cu Nanowire Synthesis by PVP-Ethylene Glycol Route. *J. Nanomater.* **2018**, *2018*, 1.
(46) Yokoyama, S.; Motomiya, K.; Jeyadevan, B.; Tohji, K. Environmentally friendly synthesis and formation mechanism of copper nanowires with controlled aspect ratios from aqueous solution with ascorbic acid. *J. Colloid Interface Sci.* **2018**, *531*, 109−118.
(47) Wang, X.; Wang, R.; Shi, L.; Sun, J. Kinetically controlled synthesis of Cu nanowires with tunable diameters and their applications in transparent electrodes. *J. Mater. Chem. C* **2018**, *6*, 1048.
(48) Tang, Z.; Kwon, H.; Yi, M.; Kim, K.; Han, J. W.; Kim, W.-S.; Yu, T. Role of Halide Ions for Controlling Morphology of Copper Nanocrystals in Aqueous Solution. *ChemistrySelect* **2017**, *2*, 4655−4661.
(49) McCrum, I. T.; Akhade, S. A.; Janik, M. J. Electrochemical specific adsorption of halides on Cu 111,100, and 211: A Density Functional Theory study. *Electrochim. Acta* **2015**, *173*, 302−309.
(50) Filankembo, A.; Giorgio, S.; Lisiecki, I.; Pileni, M. P. Is the Anion the Major Parameter in the Shape Control of Nanocrystals? *J. Phys. Chem. B* **2003**, *107*, 7492−7500.
(51) Jeong, S.; Liu, Y.; Zhong, Y.; Zhan, X.; Li, Y.; Wang, Y.; Cha, P. M.; Chen, J.; Ye, X. Heterometallic Seed-Mediated Growth of Monodisperse Colloidal Copper Nanorods with Widely Tunable Plasmonic Resonances. *Nano Lett.* **2020**, *20*, 7263−7271.
(52) Kresse, G.; Hafner, J. Ab Initio Molecular Dynamics for Liquid Metals. *Phys. Rev. B* **1993**, *47*, 558−561.
(53) Kresse, G.; Furthmüller, J. Efficiency of Ab-Initio Total Energy Calculations for Metals and Semiconductors Using a Plane-Wave Basis Set. *Comput. Mater. Sci.* **1996**, *6*, 15−50.
(54) Kresse, G.; Hafner, J. Ab Initio Molecular-Dynamics Simulation of the Liquid-Metal−amorphous-Semiconductor Transition in Germanium. *Phys. Rev. B* **1994**, *49*, 14251−14269.
(55) Kresse, G.; Furthmüller, J. Efficient Iterative Schemes for Ab Initio Total-Energy Calculations Using a Plane-Wave Basis Set. *Phys. Rev. B* **1996**, *54*, 11169−11186.
(56) Blöchl, P. E. Projector Augmented-Wave Method. *Phys. Rev. B* **1994**, *50*, 17953−17979.
(57) Kresse, G.; Joubert, D. From Ultrasoft Pseudopotentials to the Projector Augmented-Wave Method. *Phys. Rev. B* **1999**, *59*, 1758−1775.
(58) Perdew, J. P.; Burke, K.; Ernzerhof, M. Generalized Gradient Approximation Made Simple. *Phys. Rev. Lett.* **1996**, *77*, 3865−3868.
(59) Monkhorst, H. J.; Pack, J. D. Special points for Brillouin-zone integrations. *Phys. Rev. B* **1976**, *13*, 5188−5192.

https://doi.org/10.1021/acsomega.2c00359
ACS Omega 2022, 7, 7414−7420